STRUCTURAL PARAMETERS STUDY ON STAINLESS-STEEL FLAT-TUBE HEAT EXCHANGERS WITH CORRUGATED FINS

by

Guifeng GAO[a*], Fei WANG[b,c], and Yongzhang CUI[d]

[a]College of Architecture Engineering, Shandong Yingcai University, Jinan, Shandong, China
[b]Zhejiang Health Intelligent Kitchen System Integration Key Laboratory, Ningbo, China
[c]Ningbo Fangtai Kitchenware Co., Ltd., Ningbo, China
[d]College of Thermal Energy Engineering, Shandong Jianzhu University, Jinan, Shandong, China

Original scientific paper
https://doi.org/10.2298/TSCI191105008G

A stainless steel corrugated fins and flat-tube heat exchanger is designed, which has a plate-fin structure. To optimize the structural parameters of this exchanger, including corrugation angle, corrugation pitch and fin length, 3-D simulation model and test were proposed. The numerical results indicated that the corrugation angle significantly affects both on heat transfer performance and pressure drop. The fin with angle, A = 0~20°, have demonstrated the higher heat transfer efficiency, lesser gas condensation, lower pressure drop, higher outlet flue gas temperature in low T region, and no exceeding the distortion temperature in high T region. Corrugation pitch and fin length influence thermal and hydraulic characteristics, outlet flue gas temperature, and fin temperature. To improve heat transfer performance, and reduce the fin temperature in high T region and ease gas condensation in low T region, smaller corrugation pitch and shorter fin length were recommended in the low T region, whereas higher values were more reasonable in high T region. Noticeably, the heat transfer and flow characteristics were better in the high T region than the low T region. Therefore, higher priority should be given to the structural optimization in the high T region in order to increase the heat transfer enhancement.

Keywords: *flat-tube heat exchange, corrugated fin, corrugation angle, corrugation pitch*

Introduction

Gas-fired water heater has been widely used in our daily life, due to its convenient use, easy construction, low cost and high reliability. The most common type of heat exchanger used in gas-fired water heater was the copper tube-fin compact heat exchanger, what consists of water tube banks and gas side fins [1]. Many individual fins were connected to the tubes by the tube expansion process [2, 3]. Nevertheless, there have several disadvantages to this structure.

Typically, in the water tube banks, there were so many water tubes whose size is narrow and small, which leads to the large resistance of water [4-7]. Besides, it usually has several rows of fined tubes. Thus, the heat transfer in the tubes is uneven. The heat transfer

*Corresponding author, e-mail: gaoguifeng@ycxy.com

performance in the inlet rows is the best, and it in the outlet becomes worse gradually. Low temperature corrosion would arise in the low temperature outlet rows, especially in the low flue temperature, low air coefficient, and cold water temperature [8]. Thirdly, the thermal contact resistance existed in the tub-fin heat exchangers [9], which also lead to the heat transfer efficiency decrease. Fourthly, the price of the copper heat exchanger was higher than other materials, such as aluminum and casting aluminum-silicon alloy, carbon steel, stainless steel and polymer heat exchanger [10, 11].

To resolve the problems, a stainless steel corrugated fins, and flat-tube heat exchanger is designed. Different from the conventional heat exchanger, it has a plate-fin structure [12-14], which was common in plate heat exchangers but is rare in gas tubular heat exchangers. The flat-tube structure is used to accommodate the corrugated fins. Since the sectional area of the flat-tube is large, it became possible to increase the heat transfer ribs in the tubes [15-17]. Otherwise, stainless steel, as a corrosion-resistant material, was selected in this study, and it also can reduce product cost.

The Qi *et al*. [17] and Sanderby [18] studied corrugated fins and flat-tube heat exchanger, in which they found fin pitch, fin thickness, and fin angle influence significantly the performance of the heat exchanger. They used multi-louvered fins to enhance heat transfer. However, this exchanger was used in compact heat exchangers of the refrigeration and air conditioning systems. A series of numerical and experimental investigations [19-28] based on various tubes, such as an elliptical, circular, external extended finned tube, plain finned-tube, and wavy finned-tube heat exchanger, offset strip finned-tube heat exchanger, louvered finned-tube, were used to enhance heat transfer. In these numerical investigations, the models, such as SST k-ε, RNG k-ε, CRB-STHX, and HCB-STHX, were used.

The design exchanger, named as corrugated fins and flat-tube heat exchanger, consists of flat tubes and corrugated fins, as shown in fig. 1. The working mechanism can be illuminated as follows. Water flowed in the parallel tubes, and gas flowed in the fin channels. The heat exchanger used in a gas-fired water heater could be divided into the high temperature region and low temperature region. The high T region was at the gas inlet and the low T region was at the outlet. The corrugated fins and flat-tube heat exchanger can be used as high temperature heat exchangers in the high T region and as low temperature heat exchangers in the low T region. In addition to being used in gas water heaters, it also can be used in high temperature flue gas environment as a super heater in the low-capacity boiler, and used in low temperature flue gas environment as an economizer.

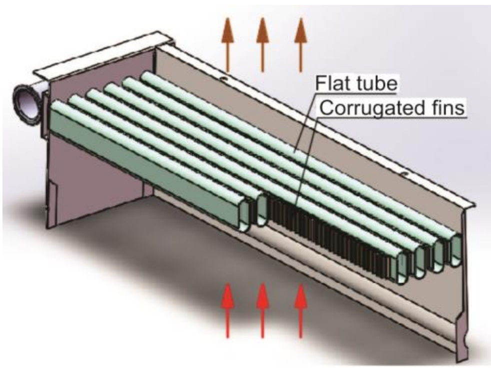

Figure 1. Corrugated fins and flat-tube heat exchanger

In the process of working, the following two defects should be paid attention to. First, in the high T region, the fins deformation would occur if the fin temperature exceeds the distortion value. Second, in the low T region, flue gas condensation would be unavoidable if the fin temperature below the condensation value. The deformation and gas condensation were eliminated in this investigation.

In this study, a 3-D simulation model was developed, and the numerical simulations were carried out with different corrugation angles, corrugation pitches, and fin lengths in order to optimize the structure parameters of stainless steel corrugated fins and flat-tube heat exchanger, to enhance heat transfer efficiency, and to eliminate the deformation and to ease gas condensation. The flow structure and field distribution were analyzed. The effects of corrugation angle, corrugation pitch, and fin length were detailed. Finally, optimized structure parameters were proposed in this paper.

Mathematical analysis

Governing equations

The numerical simulation was carried out using FLUENT, with RNG κ-ε, SIMPLE pressure-velocity coupling algorithm, and the second upwind discretization scheme for momentum, energy, turbulent kinetic energy, and dissipation energy. Under-relaxation factors of turbulent kinetic energy, turbulent dissipation rate, and turbulent viscosity were changed within the range between 0.2 and 0.4, others taken the default values. For accounting for the low Reynolds number and the near wall flow, an enhanced wall treatment was also adopted.

The governing equations of flow and heat transfer including steady-state mass, momentum, and energy conservation equations, [29-31]:

$$\frac{\partial \rho}{\partial t}+\frac{\partial}{\partial x_i}(\rho u_i)=0 \tag{1}$$

$$\frac{\partial}{\partial t}(\rho u_i)+\frac{\partial}{\partial x_j}(\rho u_i u_j)=-\frac{\partial p}{\partial x_i}+\frac{\partial}{\partial x_j}\left[\mu\left(\frac{\partial u_i}{\partial x_j}+\frac{\partial u_j}{\partial x_i}-\frac{2}{3}\delta_{ij}\frac{\partial u_l}{\partial x_l}\right)\right]+\frac{\partial}{\partial x_j}\left(-\rho\overline{u_i^{'}u_j^{'}}\right) \tag{2}$$

$$\frac{\partial}{\partial x_j}\rho C\left(u_j T\right)=u_j\frac{\partial P}{\partial x_j}+\overline{u_j^{'}\frac{\partial P'}{\partial X_j}}+\frac{\partial}{\partial x_j}\left(\lambda\frac{\partial T}{\partial x_j}-\rho C\overline{u_j^{'}T^{'}}\right) \tag{3}$$

Turbulent kinetic equation:

$$\frac{\partial}{\partial t}(\rho k)+\frac{\partial}{\partial x_i}(\rho k u_i)=\frac{\partial}{\partial x_j}\left(\alpha_k\mu_{\text{eff}}\frac{\partial k}{\partial x_j}\right)+G_k+\rho\varepsilon \tag{4}$$

Computational models

The structure of the flat-tube heat exchanger was shown in fig 2. The exchanger has four structural parameters: corrugation angle (A), tube pitch (B), corrugation pitch (D), and fin length (H). The H was equal to the horizontal length of the flat tube. Specifically, A, D, and H were the key parameters.

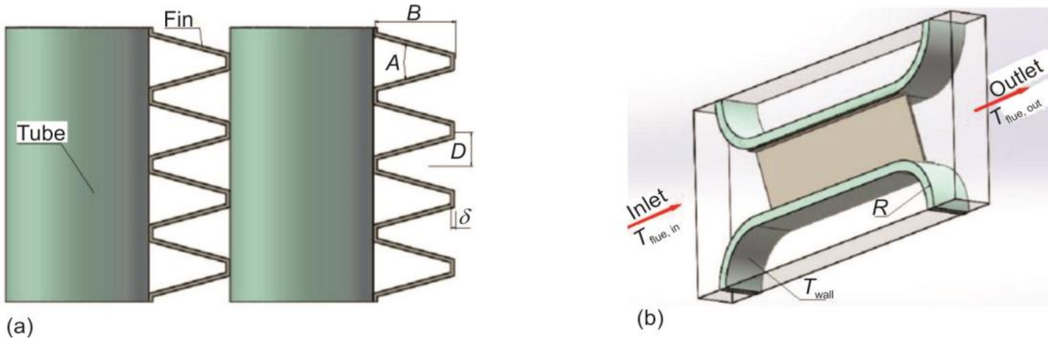

Figure 2. (a) Heat exchanger structural parameters, (b) the3-D computational domain

To simplify numerical simulation and maintain the basic characteristics of the process, the following assumptions were made [32, 33]. Firstly, natural-convection heat transfer, flame radiation, and smoke radiation were ignored. Secondly, viscous heating was neglected due to limited fluid velocity and incompressible medium. Thirdly, the changes in flue gas composition and physical properties were ignored. Finally, a constant temperature was assumed for solid walls. Based on these assumptions, a flow unit channel of corrugated fins was taken as a simplified model for the flue gas side, in order to perform the numerical simulations.

The boundary conditions of the computational domain were selected based on the physical operating conditions of the heat exchanger. No-slip condition was applied on tube and fin surfaces. To simplify calculations, no simulation was performed on the fluid flow in the tubes when comparing fins to each other. In this case, constant wall temperature T_w = 350 K in higher T region and T_w = 325 K in low T region in tubes inner wall were set for solid surface. The mass inlet boundary condition is applied to the gas inlet. The pressure outlet boundary was set to atmospheric pressure at the gas outlet. Coupled wall condition was set for fin surfaces and the outer wall of tubes. The thermal conductivity of tubes was set for the value of stainless steel 316 L. The temperature of inlet flue gas was set as 1300 K in the high T region, while 550 K in the low T region. Problem geometry dimensions and operating conditions are summarized in tab. 1.

Table 1. Details of computational geometry and operating conditions

Parameter	Value A	Value D	Value H
Corrugation angle A [°]	0, 10, 20, 30, 40	0	0
Tube pitch, B [mm]	1.99	1.99	1.99
Corrugation pitch, D [mm]	2.06	1.66, 2.06, 2.46, 2.86, 3.26	2.06
Fin length, H [mm]	13	13	12,13,14,15,16
Thickness, δ [mm]	0.2	0.2	0.2
Tube external diameter, d [mm]	7	7	7
Reynolds number	355~358 (high T) 653~658 (low T)	422, 358, 311, 275 247	368, 358, 348, 340 333
Mass-flow rate, G_c [kgm^{-2}s^{-1}]	0.846	0.846	0.846
Flue gas inlet temperature, $T_\mathrm{flue,in}$ [K]	1300 (high T) 550 (low T)	1300	1300
Inner wall temperature, T_w [K]	350 (high T) 325 (low T)	350	350

Data reduction

Heat transfer characteristics were determined using several parameters, such as fin coefficient, θ, fin efficiency, η_fin, heat transfer and flow performance ratio, η. These parameters could be calculated [34, 35]:

$$\theta = \frac{F_{G-\mathrm{fin}} + F_{G-\mathrm{tube}}}{F_{G-\mathrm{tube}}} \tag{5}$$

$$\eta_{in} = \frac{Q_\mathrm{fin} + Q_\mathrm{tube}}{Q_\mathrm{tube}\theta} \tag{6}$$

$$\Delta T_m = \frac{\left(T_{\text{flue,in}} - T_\text{w}\right) - \left(T_{\text{flue,out}} - T_\text{w}\right)}{\ln\left(\dfrac{T_{\text{flue,in}} - T_\text{w}}{T_{\text{flue,out}} - T_\text{w}}\right)} \tag{7}$$

$$D_h = \frac{4\left[F_c H + D\left(Bd + d^2 - \dfrac{1}{8}\pi d^2\right)\right]}{F_0} \tag{8}$$

where

$$F_c = BD - \delta\left[D - \delta - \left(B - \delta\right)\tan\left(\frac{1}{2}A\right)\right] - B\delta\cos\left(\frac{1}{2}A\right)$$

$$F_0 = \left[2D - 2\delta + 2\left(B - \delta\right)\cos\left(\frac{1}{2}A\right)\right]H + \pi dD$$

The Nusselt number is defined:

$$\text{Nu} = \frac{h_o D_h}{\lambda} = \frac{QD_h}{F_0 \Delta T_m \lambda} \tag{9}$$

The friction factor, f, is calculated [35]:

$$f = \frac{F_c}{F_0}\frac{\rho_m}{\rho_i}\left[\frac{2\Delta P \rho_i}{G_c^2} - \left(1 + \sigma^2\right) - \left(\frac{\rho_i}{\rho_0} - 1\right)\right] \tag{10}$$

where

$$\sigma = \frac{F_c}{F_{fr}}, \quad F_{fr} = \left(d + B\right)D$$

Heat transfer and flow performance ratio, η, is defined:

$$\eta = \frac{\dfrac{\text{Nu}}{\text{Nu}_0}}{\left(\dfrac{f}{f_0}\right)^{1/3}} \tag{11}$$

The Reynolds number based on the frontal flow inlet velocity and fin length is defined:

$$\text{Re} = \frac{\rho u_c D_h}{\mu} \tag{12}$$

Grid independence and validation of the mathematical models

Grid independency

Mesh independence study was carried out at a corrugation angle of 20°, corrugation pitch of 2.06 mm, tube pitch of 1.99 mm and the fin length of 13 mm. in the present research. The mesh was refined starting from 0.82 to 5.91 million elements. In particular, the models of 0.82, 1.78, 3.56 and 5.91 million elements were tested. The results of the outlet temperature were evaluated for the mesh independence study. Differences between the temperature values of 5.91 million elements model and those of 0.82, 1.78, and 3.56 million elements models were 2.1, 0.1, and 0.003%, respectively. Finally, a total of 1.78 million elements were used to solve the computational flow domain, and the near-wall mesh computed heat flux more precisely. The criterion of convergence was achieved for each calculation if all variable residuals $<1.0 \times 10^{-4}$.

The numerical model validation

Test apparatus and experimental method

To validate the effectiveness of the mathematical model, the following experiments were carried out. The exchanger structure that was illuminated in fig. 3 was the same as the geometry listed in tab. 1. Different materials were selected for heat exchanger, in which the material of flat tubes was stainless steel 316 L and the material of corrugated fins was stainless steel 310S. A cooler was assigned on flue gas inlet to ensure the flow distribution and temperature control. Five thermocouples were used to measure the average temperatures of inlet flue gas. The average inlet temperature, $T_{\text{flue, in}}$, was regulated around the given values by adjusting the cooler. To obtain an average outlet flue gas temperature, $T_{\text{test, flue, out}}$, five thermocouples were uniformly placed at the outlet. Mass-flow rate was determined by adjusting the amount of natural gas. Gas volume and composition were measured by gas flow-meter and smoke analyzer, respectively. After obtaining gas volume and composition, the mass-flow rate was calculated.

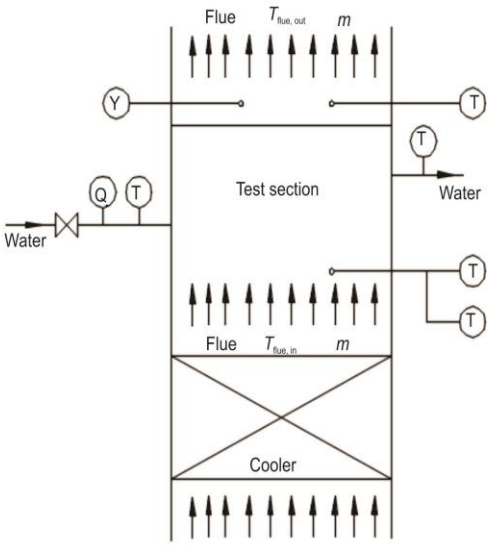

Figure 3. The testing system of the heat exchanger

The water system proposed of small temperature difference (1°) with large water flow rate was used to ensure that T_w was around the given values. Two thermal resistance thermometers were used to measure both inlet and outlet water temperatures, respectively. A water flow-meter was assigned to the inlet water pipe. Meanwhile, two surface thermal resistance thermometers were used to measure the inner surface temperature of flat tubes, T_w.

Two groups of experiments were taken based on the apparatus: high T region test, $T_{\text{flue,in}}$ = 1300 K and low T region test $T_{\text{flue,in}}$ = 550 K. Details of computational geometry and operating conditions are given in tab. 2.

Model validation

To further ensure the accuracy of the present numerical simulation, the calculated results were compared with the experimental results. Results of comparison had been illustrated in fig. 4. A good agreement between the present numerical results and the theoretical results was observed, and the maximum relative error was within 1.5%, indicating the current numerical method was reliable.

Table 2. Details of structure parameters and test conditions

Parameter	Value of high T region test	Value of low T region test
Corrugation angle, A [°]	0, 10, 20, 30, 40	0, 10, 20, 30, 40
Tube pitch, B [mm]	1.99	1.99
Corrugation pitch, D [mm]	2.06	2.06
Fin length, H [mm]	13	13
Thickness, δ [mm]	0.2	0.2
Tube external diameter, d [mm]	7	7
Reynolds number	355~358	653~658
Mass flow rate, G_c [gm^{-2}s^{-1}]	0.846	0.846
Flue gas inlet temperature, $T_{\text{flue,in}}$ [K]	1300±5	550±2
Inner wall temperature T_{w} [K]	350±1	325±1

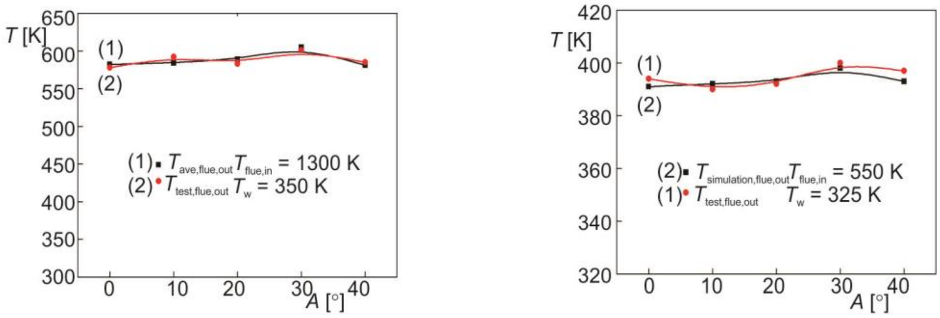

Figure 4. Comparison between $T_{\text{simulation,flue,out}}$ and $T_{\text{test,flue,out}}$

Results and discussion

The effects of the selected parameters on the heat transfer and flow characteristics in two working conditions, high T region and low T region, were investigated by numerical method.

Corrugation angle, A

To recognize fin angle, A, effects on heat transfer and flow characteristics, all fin types including A = 0°, 10°, 20°, 30°, and 40° were compared to each other. As shown in fig 5, it was worth noting that with A increased, Q_{fin} first decreased and then increased, whereas Q_{tube} first increased and then decreased, in both high T region and low T region. Meanwhile, Q first decreased and then increased, and the smallest was occurred at A = 30°. Figure 6 shows that the average outlet flue gas temperatures ($T_{\text{ave.flue.out}}$) and fin temperatures ($T_{\text{ave.fin}}$) first increased and then decreased in both high T region and low T region, and the largest increase occurred at A = 30°.

As shown in fig. 7, it was observed that fin efficiency, η_{fin}, first decreased and then increased in both high T region and low T region, and the smallest increase occurred at A = 30°. The η of the high T region was higher compared with that of the low T region. Thus, higher priority should be given to structural optimization in the high T region in order to improve the heat transfer rate. According to fig. 8, with increasing A, the F_{fin} and F were first decreased and then increased, and the smallest increase was observed at A = 30°.

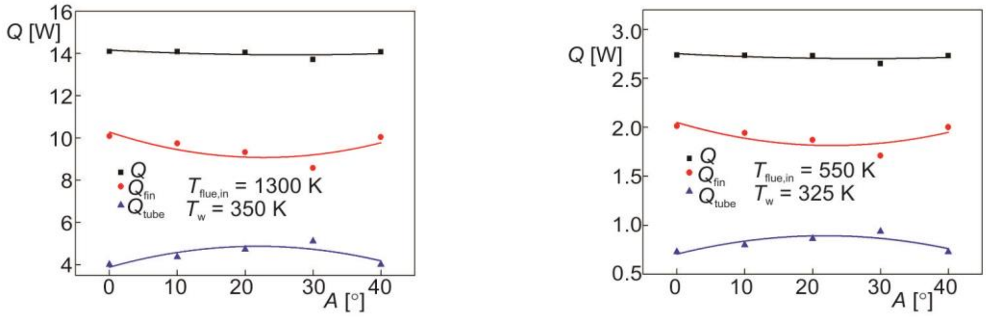

Figure 5. Heat transfer rates *vs*. corrugated angles

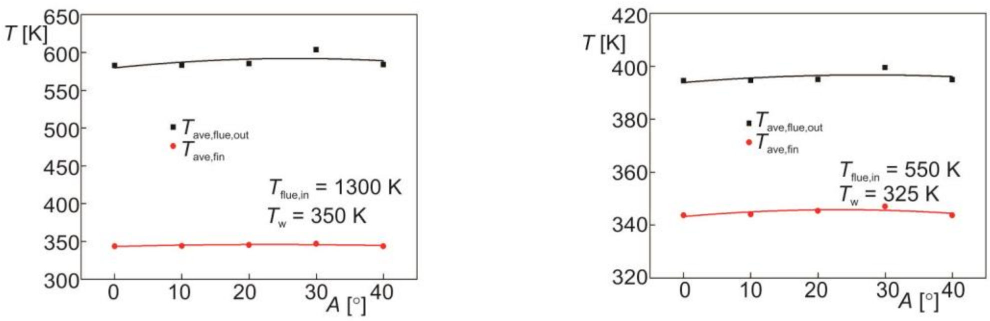

Figure 6. Average temperatures *vs*. corrugation angles

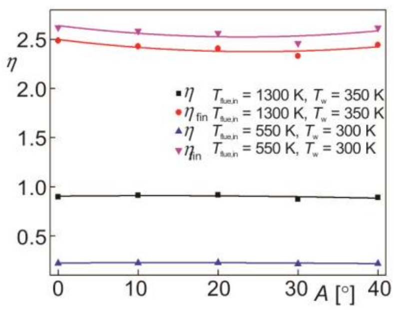

Figure 7. Fin efficient and η

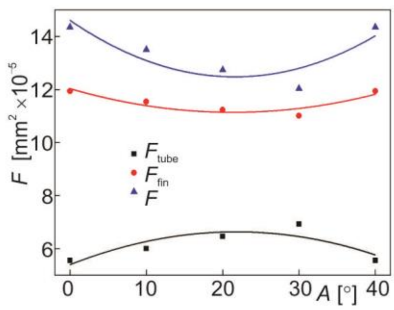

Figure 8. Areas *vs*. corrugated angles

Overall, as increasing A, Q_{fin}, Q, and T were first decreased and then increased, whereas η_{fin} was first decreased and then increased. The variation of F is the reason for the trend of other parameters Q_{fin}, Q , T ,η_{fin}, and η.

The results, such as F, Q, η_{fin}, and T, also could be explained by the facts presented in fig. 9. Velocity contours were obtained from the inlet, middle and outlet of the flow channel minimum cross-section planes at different angles, fig. 9. It was noted that, as the flue gas entered the channel, a thicker velocity boundary layer was formed. With increasing *A*, the layer thickness increased gradually. However, at $A = 30°$ and 40°, higher thickness of velocity boundary-layer led to a velocity blind zone in the corner. Notably, the layer thickness was increased from inlet to outlet at the same angle. The inlet blind area resulting in a worse overall heat transfer performance was smallest compared with outlet and middle. The $A = 0°$ blind area, in which the fin area was non-effective, was smallest compared with $A = 20°$, 30°, and 40°.

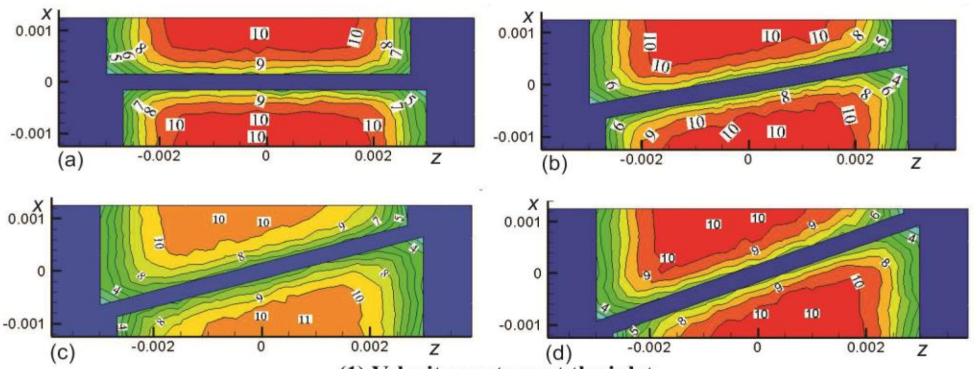

(1) Velocity contour at the inlet

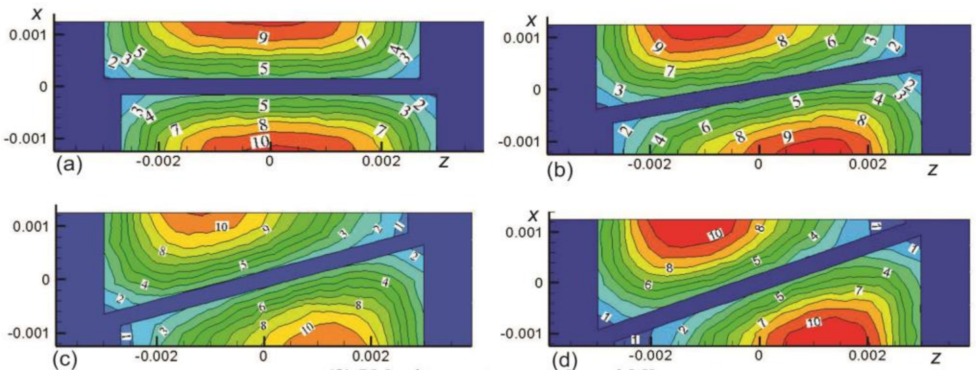

(2) Velocity contour at the middle

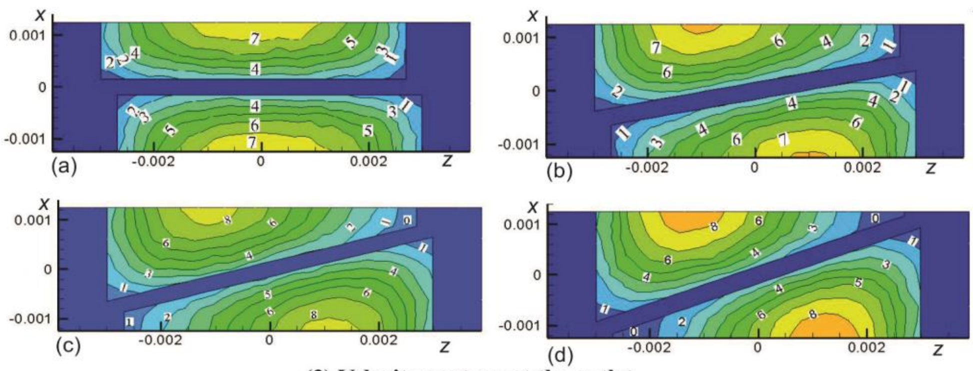

(3) Velocity contour at the outlet

Figure 9. Velocity contour on the *x*-z plane; (a) $A = 0^o$, (b) $A = 20^o$, (c) $A = 30^o$, and (d) $A = 40^o$

Combine that with another phenomenon that is as the A increases the fins geometric area increases, so fig. 8, with A increased F first decreased then increased and the smallest increase observed at A = 30°, could be verified. It was also worth noting that in blind zone corner of low T region outlet area, especially in which A = 30° and 40°, might suffer gas condensation. It was summarized that the larger the A, the more material consumption and the less economic, so smaller A, as A = 0~20°, should be used in this structural.

In fig. 10(a), the highest fin temperature was approximately 680 K in the high T region, which was lower than the distortion temperature of stainless-steel 310S (approximately 1073 K). It was worth noting that the lowest fin temperature in the low T region was occurred in the outlet of the fin corner as shown in fig. 10(b). It can be concluded that the fin structure of angle A = 0° could ease the corrosion, but could not eliminate it.

Besides, the pressure drop of A = 30° was 2.5 Pa smaller than that of A = 0° in the high T region, whereas 1.5 Pa smaller in the low T region, fig. 11. These results indicate that fin angle variation does not offer a significant effect on pressure drop.

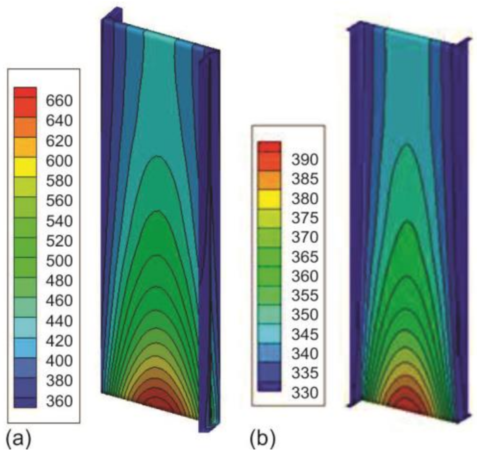

Figure 10. Temperature contours;
(a) Fin *T* contours in high *T* region from *A* = 0°
(b) Fin *T* contours in low *T* region from *A* = 0°

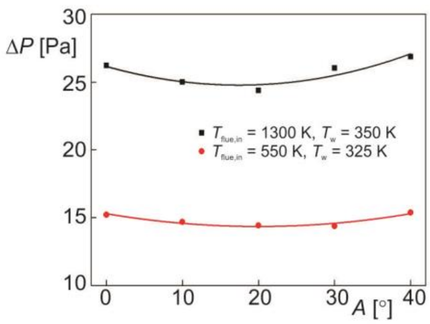

Figure 11. Pressure drop *vs.* corrugation angles

In short, smaller A, as A = 0~20°, has demonstrated the higher heat transfer efficiency, lesser gas condensation, lower pressure drop, higher outlet flue gas temperature in low T region, and no exceeding the distortion temperature in high T region. Fourth more, it was found that the heat transfer rate and flow performance ratio, η, were obviously higher in the high T region than the low T region. Thus, higher priority should be given to the structure optimization in the high T region in order to improve the heat transfer rate. Thus, higher priority should be given to the structure optimization in the high T region in order to improve the heat transfer rate.

Fin length H

As the fin length increased from 12 to 16 mm in the high T region, F_{fin} increased by approximately 20%, and the pressure drop increased the number of 0.5 Pa. These results suggest that the influence of H on pressure drop is little. With H increased, Q and Q_{fin} were increased approximately 8.5% and 12%, respectively, fig. 12. In this case, because of H increased, the length of the flue gas tunnel increased, which resulted in the heat transfer performance enhancement and $T_{\text{ave,flue,out}}$ significantly decreased from 600 to 535 K while $T_{\text{ave,fin}}$ decreased to 19 K. However, as shown in fig. 13, with H increased in the low T region, the low temperature of the outlet might lead to gas condensation.

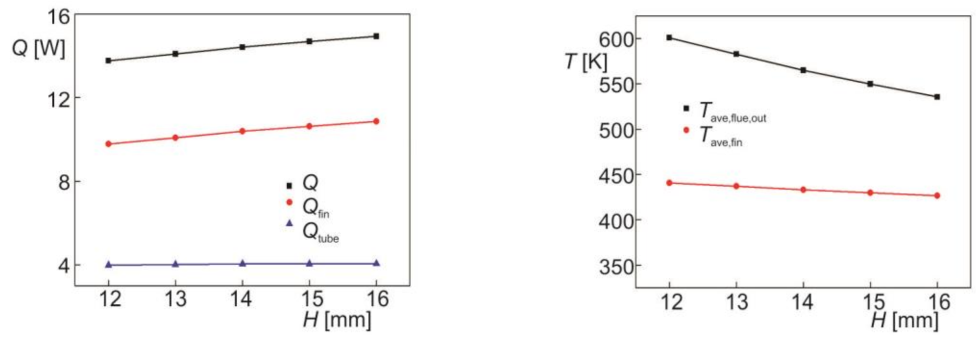

Figure 12. Heat transfer rate (a) and temperature (b) *vs.* fin height.

Overall, it can be concluded that H affects heat transfer rate, outlet flue gas temperature, and fin temperature. These data has indicated that fin length should be kept a smaller value in low T region to improve the outlet flue gas temperature and to ease gas condensation, and in high T region kept a larger value to enhance heat transfer performance and reduce the fin temperature.

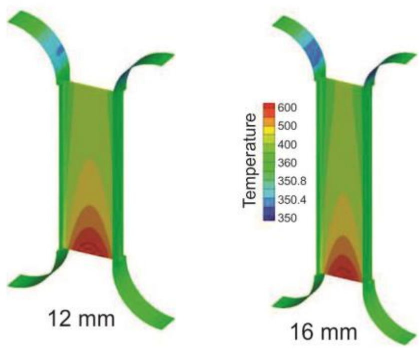

Figure 13. Temperature distribution of outer tube and fin with different fin height

Corrugation pitch D

As fin pitch D increased from 1.66 to 3.26 mm in high T region, θ decreased from 2.4 to 1.9 and η_{in} decreased from 2.7 to 1.95, figs. 14 and 15. Such decreases caused a significant increase in outlet temperature T_{flueout} from 585 to 793 K. Besides, η was in-

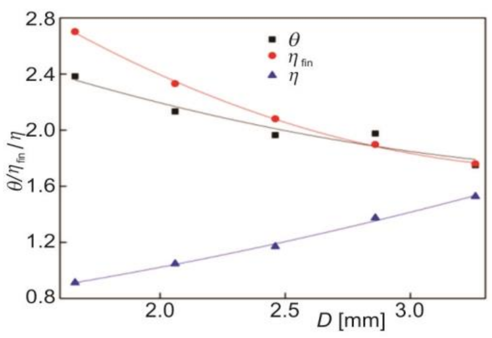

Figure 14. Fin coefficient and efficient *vs.* corrugation pitch

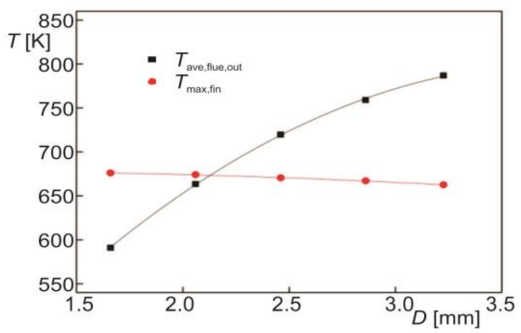

Figure 15. Gas and fin temperatures vs. corrugation pitch

creased from 0.8 to 1.6, while $T_{\text{fin,max}}$ decreased slightly approximately 20 K. This can the mass by the fact that the flow channel minimum cross-section area increased due to increasing *D*, leading to a reduction of flue gas velocity. It can be concluded that *D* determine the heat transfer rate, outlet flue gas temperature and fin temperature. These data indicate that fin pitch should be kept a smaller value in low *T* region to elevate the outlet flue gas temperature and kept a larger value in high *T* region to enhance heat transfer performance to reduce the fin temperature.

Conclusion

This study reveals the structure parameters optimization of stainless steel corrugated fins and flat-tube heat exchanger. Numerical simulations were performed with different corrugation angles, corrugation pitches, and fin lengths to enhance heat transfer and pressure drop characteristics in high and low temperature conditions. The conclusions are as follows.

- The corrugation angle significantly affects both thermal and flow characteristics. The fins with $A = 0\sim20°$, have demonstrated the higher heat transfer efficiency, lesser gas condensation, lower pressure drop, higher outlet flue gas temperature in low *T* region, and no exceeding the distortion temperature in high *T* region.
- The heat transfer rate and flow performance ratio, η, were higher in the high *T* region than the low *T* region. Thus, higher priority should be given to the structure optimization in high *T* region in order to improve the heat transfer rate.
- Corrugation pitches and fin length influence the effects of heat transfer rate, fin temperature, and outlet flue gas temperature. It is worth noting that smaller values of fin pitch and height are suitable in the low *T* region, whereas larger values are more reasonable in the high *T* region.

Acknowledgment

The work is supported by the Specialized Research Fund of Fangtai Kitchenware Co., Ltd.

Nomenclature

A	– corrugation angle, [°]
B	– tube pitch, [mm]
D	– corrugation pitch, [mm]
D_h	– hydraulic diameter, [m]
d	– tube external diameter, [mm]
F_0	– total outside surface area, [m^2]
F_c	– minimum flow area, [m^2]
F_{fr}	– inlet frontal flow area, [m^2]
F_{fin}	– fin effective heat transfer area, [m^2]
$F_{\text{G-fin}}$	–fin geometric surface area, [m^2]
$F_{\text{G-tube}}$	– tube geometric surface area, [m^2]
F_{tube}	– tube effective heat transfer area, [m^2]
f	– friction factor
f_0	– *f* based on tube without any fin
G_c	– mass flux at minimum flow area (kgm^{-2}s^{-1})
H	– fin length, [mm]
h_0	– heat transfer coefficient, [Wm^{-2}K^{-1}]
Nu	– Nusselt number
Nu$_0$	– Nu based on tube without any fin
ΔP	– pressure drop, [Pa]
Q	– total heat transfer rate, [W]
Q_{fin}	– fin heat transfer rate, [W]
Q_{tube}	– tubes heat transfer rate, [W]
Re	– Reynolds number
$T_{\text{ave,flue,out}}$	– average temperature of outlet flue gas [K]
$T_{\text{ave,fin}}$	– average temperature of fin, [K]
$T_{\text{flue,in}}$	– inlet temperature of flue gas, [K]
$T_{\text{flue,out}}$	– outlet temperature of flue gas, [K]
T_{w}	– inner wall temperature of tube, [K]
ΔT_{m}	– log-mean temperature difference, [K]
u_c	– velocity at the minimum cross-sectional area, [ms^{-1}]

Greek symbols

α_k	– inverse effective Prandtl numbers for *k*
δ	– thickness, [mm]
ρ	– density, [kgm^{-3}]
ρ_m	– mean density, [kgm^{-3}]
ρ_i	– inlet density, [kgm^{-3}]
ρ_0	– outlet density, [kgm^{-3}]
η	– heat transfer and flow performance ratio
η_{fin}	– fin efficiency

θ – fin coefficient
λ – thermal conductivity, [$\mathrm{Wm^{-1}K^{-1}}$]
μ – dynamic viscosity, [$\mathrm{kgm^{-1}s^{-1}}$]

References

[1] Zhang, G. H., *et al.,* Review of Experimentation and Modeling of Heat and Mass Transfer Performance of Fin-and-Tube Heat Exchangers with Dehumidification, *Appl. Therm. Eng., 146* (2019), Jan., pp. 701-717
[2] Ahmadali, G., Hussein, A. Mohammed Parametric Design Exploration of Fin-and-Oval Tube Compact Heat Exchangers, *International Journal of Thermal Sciences, 144* (2019), Oct., pp. 173-190
[3] Tang, D., *et al.,* Optimization to the Tube-Fin Contact Status of the Tube Expansion Process, *Journal of Materials Processing Technology, 211* (2011), 4, pp. 573-577
[4] Abdulkerim, O., *et al.,* An Experimental, Computational and Flow Visualization Study on the Air-Side Thermal and Hydraulic Performance of Louvered Fin and Round Tube Heat Exchangers, *International Journal of heat and mass transfer*, *121* (2018), June, pp. 153-169
[5] Sajedi, R., *et al.,* Experimental and Numerical Study on the Optimal Fin Numbering in an External Extended Finned Tube Heat Exchanger, *Applied Thermal Engineering, 83* (2015), May, 139e146
[6] Malapure, V. P., *et al.,* Numerical Investigation of Fluid Flow and Heat Transfer Over Louvered fins in Compact Heat Exchanger, *Int. J. Therm. Sci. 46* (2007), 2, pp. 199-211
[7] Arafat, A. *et al.,* Thermal and Hydraulic Performance of Finned-Tube Heat Exchangers Under Different Flow Ranges: A Review on Modeling and Experiment, *International Journal of Heat and Mass Transfer, 101* (2016), Oct., pp. 38-59
[8] Xu, J., *et al.,* Numerical Simulation of the Flow and Heat-Transfer Characteristics of an Aligned External Three-Dimensional Rectangular-Finned Tube Bank. *Appl. Therm. Eng. 145* (2018), Dec., pp. 110-122
[9] Cao, W. X., *et al.,* Performance of Casting Aluminum-Silicon Alloy Condensing Heating Exchanger for Gas-Fired Boiler. *Heat and Mass Transf., 54* (2018), 7, pp. 1951-1960
[10] Jan, W., Mikielewicz, D.. Influence of Metallic Porous Microlayer on Pressure Drop and Heat Transfer of Stainless Steel Plate Heat Exchanger, *Applied Thermal Engineering, 93* (2016), Jan., pp. 1337-1346
[11] Lee, S. B., *et al.,* Improved Corrosion Resistance and Interfacial Contact Resistance of 316L Stainless-Steel for Proton Exchange Membrane Fuel Cell Bipolar Plates by Chromizing Surface Treatment, *Journal of Power Sources*, *187* (2009), 2, pp. 318-323
[12] Gonzalez, A. M., *et al*., A Hybrid Numerical-Experimental Analysis of Heat Transfer by Forced Convection in Plate-Finned Heat Exchangers. *Appl. Therm. Eng., 148* (2019), Feb., pp. 363-370
[13] Ismail, M. F., *et al.,* Numerical Simulation of Turbulent Heat Transfer from Perforated Plate-Fin Heat Sinks, *Heat Mass Transf, 50* (2013), 4, pp. 509-519
[14] Thamir, K. I., *et al.,* Experimental Study on the Effect of Perforations Shapes on Vertical Heated Fins Performance Under Forced Convection Heat Transfer, *International Journal of Heat and Mass Transfer*, *118* (2018), Mar., pp. 832-846
[15] Cui, Y. Z., *et al.,* 3D Numerical Simulation of Fluid Flow and Heat Transfer in a Circular Tube with Edge-Fold-Twisted-Tape Insert, *Journal of Shandong University (Engineering Science)*, *40* (2010), 2, pp. 143-148
[16] Zheng, N. B., *et al.,* Numerical Simulation and Sensitivity Analysis of Heat Transfer Enhancement in a Flat Heat Exchanger Tube with Discrete Inclined Ribs, *International Journal of Heat and Mass Transfer*, *112* (2017), Sept., pp. 509-520
[17] Qi, Z. G., *et al.,* Parametric Study on the Performance of a Heat Exchanger with Corrugated Louvered Fins, *Applied Thermal Engineering, 27* (2007), 2-3, pp. 539-544
[18] Sanderby, S. K., Mirhosseini, M., Thermal-Hydraulic Performance of a Corrugated Cooling Fin with Louvered Surfaces, *Energy Procedia, 142* (2017), Dec., pp. 4077-4084
[19] Zeeshan, M., *et al.,* Numerical Study to Predict Optimal Configuration of Fin and Tube Compact Heat Exchanger with Various Tube Shapes and Spatial Arrangements, *Energy Conversion and Management, 148* (2017), Sept., pp. 737-752
[20] Sandar, Mon M. S., Gross, U., Numerical Study of Fin-Spacing Effects in Annular-Finned Tube Heat Exchangers, *International Journal of heat and mass transfer, 47* (2004), 8-9, pp. 1953-1964
[21] Zhao, L. P., *et al.,* Parametric Study on Rectangular Finned Elliptical Tube Heat Exchangers with the Increase of Number of Rows, *International Journal of Heat and Mass Transfer, 126* (2018), Part A, pp. 871-893

[22] Wang, Q., *et al.*, Analysis on Thermal Hydraulic Performance of the Elliptical Tube in the Finned-Tube Heat Exchanger by New Method. *Int. J. Heat and Mass Trans.*, *134* (2019),May, pp. 388-307
[23] Ke, L. I., *et al.*, Sensitivity and Stress Analysis of Serrated Fin Structure in Plate-Fin Heat Exchanger on Cryogenic Condition, *International Journal of Thermal Sciences*, *145* (2019), Nov., 106013
[24] Chen, H. T., *et al.*, Numerical Simulation of Natural Convection Heat Transfer for Annular Elliptical Finned Tube Heat Exchanger with Experimental Data, *International Journal of Heat and Mass Transfer*, *127* (2018), Part C, pp. 541-554
[25] Chimres, N., *et al.*, Effect of Elliptical Winglet on the Air-Side Performance of Fin-and-Tube Heat Exchanger, *International Journal of heat and mass transfer*, *123* (2018), Aug., pp. 583-599
[26] Li, M., *et al.,* 3D Numerical Simulation of Heat and Mass Transfer of Fin-and-Tube Heat Exchanger Under Dehumidifying Conditions. *Int.J.Heat and Mass Transf., 127* (2018), Part C, pp. 597-610
[27] Sadeghianjahromi, A., *et al.*, Developed Correlations for Heat Transfer and Flow Friction Characteristics of Louvered Finned Tube Heat Exchangers, *International Journal of Thermal Sciences, 129* (2018), July, pp. 135-144
[28] Wang, Y. C., *et al.*, Turbulent Natural Convection Heat Transfer with Thermal Radiation in a Rectangular Enclosure Partially Filled with Porous Medium, *Numer. Heat Transfer A, 70* (2016), 6, pp. 639-649
[29] Delac, B., *et al.,* Numerical Investigation of Heat Transfer Enhancement in a Fin and Tube Heat Exchanger Using Vortex Generators, *Int. J. Heat Mass Transf. 78* (2014), Nov., pp. 662-669
[30] ***, ANSYS Fluent Theory Guide, 15317, 2013, pp. 724-746
[31] Qu, Y., *et al.*, Transport Capacity Analysis for Special Cross Section Heat Pipes in Radiators, *Journal of Shandong University (Engineering Science)*, *38* (2008), 5, pp. 42-46
[32] Wang, C. C., *et al.,* Sensible Heat and Friction Characteristics of PLATE FIN-and-Tube Heat Exchangers Having Plane Fins, *Int. J. Refrig. 19* (1996), 4, pp. 223-230
[33] Erek, A., *et al.,* Effect of Geometrical Parameters on Heat Transfer and Pressure Drop Characteristics of Plate Fin and Tube Heat Exchangers, *Applied Thermal Engineering, 25* (2005), 14-15, pp. 2421-2431
[34] Min, J. C., *et al.,* Calculation of Fin Efficiency of an Oval Finned Tube Heat Exchanger, *Journal of Engineering Thermophysics*, *22* (2001), 4, pp. 473-476
[35] Park, D. H., *et al.*, Study on the Heat Transfer and Fluid Flow Characteristics in V-Shaped Corrugated Composite Fin, *Applied Thermal Engineering, 102* (2016), June, pp. 293-301

Paper submitted: November 5, 2019
Paper revised: December 3, 2019
Paper accepted: December 11, 2019